Photonuclear spallation reactions in Cu

S. Shibata, M. Imamura, T. Miyachi, and M. Mutou
Institute for Nuclear Study, University of Tokyo, Tanashi, Tokyo 188, Japan

K. Sakamoto, Y. Hamajima, M. Soto, Y. Kubota, and M. Yoshida
Department of Chemistry, Faculty of Science, Kanazawa University, Kanazawa, Ishikawa 920, Japan

I. Fujiwara*
Institute of Atomic Energy, Kyoto University, Uji, Kyoto 611, Japan
(Received 10 June 1986)

Yields of 24 radioactive nuclides formed by the interaction of bremsstrahlung with maximum end-point energies of 100 MeV–1 GeV with Cu have been measured by direct γ-ray counting of irradiated targets. The yields in the mass range of 42 to 60 (except for ^{60}Cu) were analyzed by a nonlinear least-squares fit to obtain the mass yield and charge dispersion curves in spallation reactions. From the parameter values obtained, the energy dependence of the slope of the mass yield curve and the relationship between target N/Z and the most probable product N/Z were investigated and compared with the results of proton, α, and heavy-ion-induced spallation of Cu. The characteristics of photon-induced spallation are discussed.

I. INTRODUCTION

For a number of years studies of high energy spallation reactions have yielded valuable information not only for the understanding of reaction mechanisms and nuclear properties, but also for the application to other fields such as cosmic ray studies.[1] However, studies of spallation of complex nuclei by high energy photons seem to be rather scanty in comparison with those by protons. In general, the mechanism of spallation reactions has been explained on the basis of the cascade-evaporation model suggested by Serber.[2] The incident projectile initiates a knock-on cascade by the interaction with a nucleon inside the target nucleus, and a number of particles are ejected from the nucleus. The residual nucleus is deexcited by the evaporation of nucleons or nuclear clusters, and then the final product is formed.

In the case of incident photons, at higher energies than the pion production threshold ($\sim$140 MeV), the Δ isobar is probably formed inside the target nucleus by the interaction of an incident photon with a nucleon in the nucleus. This isobar decays almost immediately into a nucleon and a pion. These two particles usually develop a cascade process when they interact with other nucleons and clusters inside the nucleus. The final products are obtained after the deexcitation by particle evaporation. The initial interaction in photospallation is quite different from that in proton spallation. Therefore, it is of interest whether or not yield distribution of product nuclides is affected by this difference of the initial interaction between photon and proton incident on the same target nucleus.

In recent radiochemical studies of spallation reactions, it has been suggested that the logarithmic slope of the mass yield curve is an indirect measure of the average excitation energy transferred from the incident particles, or the temperature of the cascade residues. A smaller slope corresponds to a higher average deposition energy. In proton and heavy ion (^{14}N, ^{12}C, and ^{40}Ar) spallation reactions of Cu at $E=4$–80 GeV by Cumming *et al.*,[3–5] it has been shown that the slope decreases with the increase of the kinetic energy of incident particles up to $\sim$2 GeV and then approaches a constant value in the higher energy region, and that all of the slopes fall on the same curve. Their results indicate that different projectiles give the same distribution of the excited system.

On the other hand, the results of photon-induced spallation reactions of V (Ref. 6) and I (Ref. 7) have shown that the slope of the mass yield curve decreases with the increase of the maximum bremsstrahlung end-point energy up to 600 MeV and becomes constant in the higher energy region. This trend is apparently different from those observed in the hadron spallation reactions.

From this point of view, photon-induced spallation of Cu has been studied with bremsstrahlung in order to compare directly with the results of proton and heavy ion spallation reactions of Cu and also to confirm the trend obtained from photospallation reactions of V and I. In the present paper, we report the results by bremsstrahlung with maximum end-point energies of 100 MeV–1 GeV. The results were analyzed with the five-parameter formula given by Rudstam[8] according to Jonsson and Lindgren.[9,10] A special interest was paid to the energy dependence of the parameter P in the Rudstam's formula, to which the logarithmic slope of the mass yield curve is functionally equivalent.

II. EXPERIMENTAL PROCEDURES

The irradiations in the maximum bremsstrahlung energy region $E_{max}=300$ MeV–1 GeV were performed in

~100 MeV steps at the 1.3 GeV electron synchrotron of the Institute for Nuclear Study (INS), University of Tokyo; and those in the range $E_{max}=100$ MeV–250 MeV in ~30 MeV steps and at $E_{max}=300$ MeV were done at the 300 and 500 MeV electron linear accelerators of the Laboratory of Nuclear Science (LNS), Tohoku University, and of the Electrotechnical Laboratory (ETL), respectively.

At INS, an electron-free collimated bremsstrahlung beam from the internal target of Pt with 50 μm thickness was used, and the beam spot was about 2 cm in diameter. The Cu target and Al monitor had a size of 2.5×2.5 cm^2. Both foils had a purity of 99.99%, and their thicknesses were 450 and 270 mg/cm^2, respectively. The target stack consisted of 4–8 Cu foils and an Al foil used as an internal beam monitor. The target and monitor foils were guarded on both sides by Cu and Al foils, respectively, in order to compensate for recoil losses and to prevent cross-contamination between target and monitor.

At LNS and ETL, an uncollimated beam was obtained from the 0.5 mm thick Pt converter. The targets and monitors were cut into disks of 1 cm in diameter. Both foils were also 99.99% pure and their thicknesses were 18 and 7 mg/cm^2, respectively. These disks, including guard foils wrapped with 2 mg/cm^2 Al foil, were stacked in a quartz tube and irradiated in a water cooled target holder at LNS.[11,12] Irradiations at ETL were the same as those at LNS except for irradiating in air.

TABLE I. Relevant properties of measured nuclides.

Nuclide	Half-life	Radiation measured (keV)	Fractional abundance (%)
^{64}Cu	12.71 h	1346	0.62
^{61}Cu	3.37 h	283	13.3
		656	11.8
^{60}Cu	23.0 min	1333	87.9
		1792	45.4
^{57}Ni	36.1 h	1378	77.7
^{60}Co	5.27 yr	1173	100
		1333	100
^{58}Co	70.8 d	811	99.4
^{57}Co	271 d	122	85.6
^{56}Co	78.5 d	847	99.95
^{55}Co	17.5 h	1408	16.5
^{59}Fe	44.6 d	1099	56.5
^{56}Mn	2.58 h	1811	27.3
^{54}Mn	312.5 d	835	100
^{52}Mn	5.63 d	744	90
		1434	100
^{51}Cr	27.7 d	320	10.2
^{49}Cr	42 min	91	51.3
		153	29.2
^{48}V	15.98 d	984	100
^{48}Sc	43.7 h	1038	97.5
^{47}Sc	3.41 d	159	68.5
^{46}Sc	83.8 d	889	100
^{44}Sc^m	58.6 h	272	86.6
^{44}Sc	3.93 h	1157	99.89
^{43}K	22.3 h	373	87.8
^{42}K	12.36 h	1525	18.8
^{24}Na	15.02 h	1369	100

The absolute yields [mb per equivalent quantum (mb/eq.q)] for the monitor reaction ^{27}Al(γ,2pn)^{24}Na have already been reported by various authors.[13–18] However, the scattering of the data is appreciable. The difference between the highest and the lowest yield at the same maximum end-point energy is about 40%. Therefore, the beam intensity was also measured by means of a calibrated quantameter placed several meters behind the target stack in the irradiation of $E_{max}=850$ MeV at INS. Consequently, we adopted the data for the monitor reaction given by Johnsson *et al.*[13] as the intensity monitor, because of its agreement with the intensity measured by the quantameter within the experimental uncertainty. In other irradiations at INS, the beam intensity was monitored only by the ^{27}Al(γ,2pn)^{24}Na reaction since another target stack was always placed behind the Cu stack. At LNS, C foils were also used as a monitor by the reaction ^{12}C(γ,n)^{11}C.[19] The photon intensities were 10^8–10^9 eq.q/sec at INS and 10^{12}–10^{13} eq.q/sec at LNS and ETL, and typical irradiation times were 4 hr at INS and 5 min at LNS and ETL, respectively.

After irradiation, γ rays from Cu target foils and monitors were measured directly with pure Ge and Ge (Li) detectors with an energy resolution of 1.8 keV full width at half maximum (FWHM) at 1332 keV, connected to multichannel pulse height analyzers. The detection efficiencies of the detectors were measured by γ-ray reference sources of point size and corrected for the target or monitor thickness and the size of the beam spot by a computer program.[20] The radioactive nuclides produced in the irra-

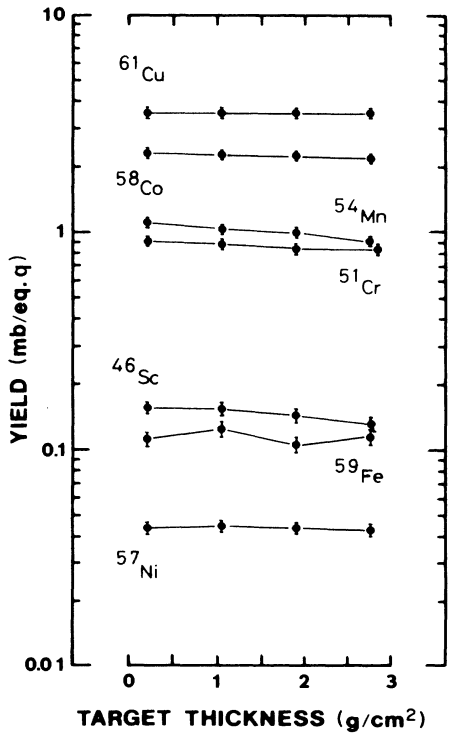

FIG. 1. Variation of some radioactivities produced in a thick Cu target stack irradiated at $E_{max}=850$ MeV.

TABLE II. Formation yield (mb/eq.q) for photon-induced spallation of Cu. Each yield is either independent (*I*) or cumulative (*C*).

Product	100 MeV	130 MeV	160 MeV	220 MeV
^{64}Cu (*I*)	15.9 ±1.1	15.9 ±0.9	16.0 ±1.0	14.8 ±1.1
^{61}Cu (*I*)	3.31 ±0.17	3.39 ±0.18	3.39 ±0.18	3.10 ±0.16
^{60}Cu (*I*)	0.199±0.018	0.217±0.019	0.217±0.018	0.256±0.030
^{57}Ni (*C*)	0.005±0.0001	0.007±0.001	0.012±0.001	0.014±0.002
^{60}Co (*I*)	0.418±0.034	0.470±0.044	0.484±0.040	0.602±0.043
^{58}Co (*I*)	0.750±0.038	0.882±0.043	0.816±0.039	1.18 ±0.06
^{57}Co (*C*)	0.256±0.013	0.341±0.017	0.352±0.018	0.570±0.029
^{56}Co (*C*)	0.035±0.002	0.053±0.003	0.068±0.004	0.133±0.007
^{55}Co (*C*)				0.023±0.005
^{59}Fe (*C*)	0.018±0.001	0.021±0.002	0.023±0.002	0.040±0.003
^{56}Mn (*C*)	0.011±0.001	0.020±0.002	0.028±0.003	0.047±0.004
^{54}Mn (*I*)	0.040±0.003	0.068±0.006	0.093±0.006	0.219±0.012
^{52}Mn (*C*)	0.002±0.001	0.004±0.001	0.009±0.001	0.034±0.002
^{51}Cr (*C*)	0.006±0.001	0.013±0.002	0.022±0.002	0.098±0.008
^{49}Cr (*C*)				
^{48}V (*C*)				0.013±0.002
^{48}Sc (*I*)				
^{47}Sc (*C*)				
^{46}Sc (*I*)				
^{44}Sc^{m} (*I*)				
^{44}Sc (*I*)				
^{43}K (*C*)				
^{42}K (*I*)				
^{24}Na (*C*)				

Product	250 MeV	305 MeV	310 MeV
^{64}Cu (*I*)	15.6 ±0.9	17.0 ±0.9	17.2 ±1.3
^{61}Cu (*I*)	3.74 ±0.21	3.54 ±0.18	3.46 ±0.18
^{60}Cu (*I*)	0.266±0.021		0.196±0.015
^{57}Ni (*C*)	0.021±0.002	0.024±0.002	0.034±0.005
^{60}Co (*I*)	0.852±0.062	0.607±0.057	0.627±0.188
^{58}Co (*I*)	1.39 ±0.07	1.28 ±0.03	1.31 ±0.07
^{57}Co (*C*)	0.726±0.037	0.766±0.016	0.826±0.062
^{56}Co (*C*)	0.169±0.009	0.185±0.006	0.230±0.027
^{55}Co (*C*)	0.023±0.004	0.031±0.006	
^{59}Fe (*C*)	0.050±0.004	0.052±0.002	0.042±0.010
^{56}Mn (*C*)	0.056±0.005	0.080±0.005	0.077±0.009
^{54}Mn (*I*)	0.308±0.017	0.388±0.005	0.480±0.069
^{52}Mn (*C*)	0.050±0.003	0.085±0.006	0.083±0.006
^{51}Cr (*C*)	0.145±0.011	0.255±0.009	0.247±0.043
^{49}Cr (*C*)			
^{48}V (*C*)	0.023±0.002	0.057±0.004	0.072±0.008
^{48}Sc (*I*)			
^{47}Sc (*C*)		0.014±0.003	0.014±0.003
^{46}Sc (*I*)		0.024±0.004	0.022±0.010
^{44}Sc^{m} (*I*)			0.012±0.002
^{44}Sc (*I*)			0.011±0.003
^{43}K (*C*)			
^{42}K (*I*)			
^{24}Na (*C*)			

Product	400 MeV	500 MeV	600 MeV	700 MeV
^{64}Cu (*I*)	16.9 ±1.2	17.4 ±1.2	16.6 ±1.0	16.5 ±1.0
^{61}Cu (*I*)	3.48 ±0.18	3.61 ±0.18	3.48 ±0.18	3.39 ±0.17
^{60}Cu (*I*)	0.220±0.015	0.209±0.013	0.228±0.013	0.218±0.012
^{57}Ni (*C*)	0.039±0.004	0.042±0.005	0.040±0.003	0.040±0.004
^{60}Co (*I*)	0.966±0.372	1.06 ±0.30	1.24 ±0.28	1.06 ±0.09
^{58}Co (*I*)	1.75 ±0.05	1.96 ±0.06	2.04 ±0.10	2.03 ±0.09

TABLE II. (*Continued*).

Product	400 MeV	500 MeV	600 MeV	700 MeV
^{57}Co (*C*)	0.986±0.013	1.25 ±0.05	1.27 ±0.04	1.32 ±0.04
^{56}Co (*C*)	0.310±0.021	0.366±0.016	0.406±0.025	0.397±0.022
^{55}Co (*C*)	0.045±0.004	0.039±0.009	0.065±0.009	0.046±0.007
^{59}Fe (*C*)	0.072±0.012	0.106±0.008	0.114±0.019	0.117±0.011
^{56}Mn (*C*)	0.103±0.009	0.145±0.010	0.151±0.010	0.154±0.009
^{54}Mn (*I*)	0.599±0.042	0.828±0.034	0.869±0.038	0.900±0.039
^{52}Mn (*C*)	0.147±0.008	0.199±0.011	0.227±0.008	0.228±0.013
^{51}Cr (*C*)	0.490±0.034	0.596±0.038	0.737±0.043	0.774±0.060
^{49}Cr (*C*)	0.031±0.005	0.043±0.004	0.051±0.005	0.052±0.004
^{48}V (*C*)	0.123±0.008	0.179±0.007	0.225±0.009	0.266±0.023
^{48}Sc (*I*)	0.009±0.002	0.017±0.003	0.018±0.002	0.015±0.003
^{47}Sc (*C*)	0.029±0.012	0.044±0.002	0.053±0.003	0.054±0.004
^{46}Sc (*I*)	0.069±0.020	0.095±0.008	0.131±0.012	0.121±0.010
^{44}Sc^{m} (*I*)	0.026±0.002	0.044±0.003	0.057±0.003	0.064±0.005
^{44}Sc (*I*)	0.024±0.003	0.043±0.005	0.051±0.005	0.058±0.007
^{43}K (*C*)			0.017±0.003	0.012±0.002
^{42}K (*I*)			0.037±0.006	0.038±0.007
^{24}Na (*C*)		0.003±0.001	0.005±0.001	0.006±0.001

Product	800 MeV	850 MeV	900 MeV	1000 MeV
^{64}Cu (*I*)	16.6 ±1.0	17.7 ±0.5	15.7 ±1.0	16.8 ±1.0
^{61}Cu (*I*)	3.60 ±0.18	3.55 ±0.09	3.38 ±0.17	3.51 ±0.18
^{60}Cu (*I*)	0.240±0.013	0.213±0.009	0.211±0.011	0.252±0.013
^{57}Ni (*C*)	0.046±0.003	0.044±0.002	0.046±0.003	0.052±0.003
^{60}Co (*I*)	1.11 ±0.13		1.14 ±0.14	1.08 ±0.16
^{58}Co (*I*)	2.04 ±0.05	2.26 ±0.06	2.26 ±0.07	2.44 ±0.08
^{57}Co (*C*)	1.34 ±0.04	1.46 ±0.04	1.40 ±0.05	1.48 ±0.05
^{56}Co (*C*)	0.403±0.018	0.367±0.010	0.448±0.017	0.495±0.022
^{55}Co (*C*)	0.070±0.008	0.057±0.003	0.061±0.010	0.070±0.009
^{59}Fe (*C*)	0.108±0.008	0.115±0.005	0.162±0.009	0.147±0.031
^{56}Mn (*C*)	0.167±0.010	0.156±0.004	0.161±0.010	0.172±0.009
^{54}Mn (*I*)	0.996±0.037	1.02 ±0.03	1.04 ±0.04	1.10 ±0.04
^{52}Mn (*C*)	0.252±0.010	0.237±0.006	0.261±0.011	0.282±0.014
^{51}Cr (*C*)	0.841±0.055	0.874±0.026	0.852±0.037	0.998±0.039
^{49}Cr (*C*)	0.057±0.004	0.057±0.003	0.054±0.003	0.061±0.004
^{48}V (*C*)	0.259±0.011	0.272±0.007	0.309±0.026	0.311±0.022
^{48}Sc (*I*)	0.016±0.001	0.015±0.001	0.023±0.002	0.029±0.002
^{47}Sc (*C*)	0.061±0.003	0.064±0.002	0.071±0.004	0.072±0.003
^{46}Sc (*I*)	0.155±0.008	0.147±0.005	0.165±0.009	0.186±0.008
^{44}Sc^{m} (*I*)	0.079±0.005	0.080±0.003	0.085±0.004	0.090±0.005
^{44}Sc (*I*)	0.069±0.007	0.067±0.005	0.070±0.006	0.073±0.007
^{43}K (*C*)	0.013±0.002	0.016±0.001		0.022±0.003
^{42}K (*I*)	0.047±0.006	0.047±0.003	0.037±0.008	0.056±0.009
^{24}Na (*C*)	0.006±0.001	0.007±0.001	0.007±0.001	0.008±0.002

diations were identified by their half-lives and energies of emitted γ rays. Their relevant properties[21] are tabulated in Table I. The measurements were continued for more than one month. The γ-ray spectra were analyzed with a peak search program[22] using the FACOM M380 computer at INS.

The contribution from secondary particles in irradiations was considered. At $E_{max}=850$ MeV, the depth profiles of radioactivities induced in the Cu stack were investigated. The results are shown in Fig. 1. In this irradiation, no serious effects were observed in the spallation yields of product nuclides. However, the yields of spallation products such as ^{54}Mn and ^{46}Sc decreased slightly with the increase of target thickness. This effect may be due to the decrease of the average energy of the incident bremsstrahlung with the increase of target thickness. Furthermore, another sample was always placed off the beam line during the irradiations, and it was found that the yield was negligibly small compared with that in the target placed in the beam line. Therefore, two or three Cu target foils placed on the upstream side to the incident photons were used in the measurements.

III. RESULTS

The measured production yields are listed in Table II. Each yield is identified as being independent (*I*) or cumu-

lative (C), and is the average of separate measurements by pure Ge and Ge(Li) detectors. These yields were calculated for the natural isotopic abundance of copper.

The errors associated with the yields refer to counting statistics, detector efficiencies of γ rays, and decay curve analyses. Systematic uncertainties due to the beam intensity calibration, which were estimated to be approximately 15%, are not included in the quoted errors. Duplicated runs were performed at $E_{max}=400$, 500, 600, 700, 900, and 1000 MeV, and their results agreed well with those listed in Table II.

In Fig. 2, the excitation functions for some isotopes that are widely separated in mass are shown. The yields of ^{61,64}Cu, the (γ,xn) reaction products, were almost constant within experimental error in the energy region of $E_{max}=100$ MeV–1 GeV. These nuclides were predominantly produced by giant resonance and quasideuteron processes induced by photons below ~ 100 MeV. The yields for products near the target mass such as ^{58}Co below the pion production threshold are also explained by the contribution from these processes. Also, the yields for spallation products at $E_{max} \leqq 250$ MeV measured at LNS are smoothly connected with those at $E_{max} \geqq 310$ MeV measured at INS. The yields at $E_{max}=305$ MeV at ETL seem to be consistent with those at $E_{max}=310$ MeV at INS. Therefore, the results show the consistency between the yields from the linear accelerators and those from the synchrotron. The present yields are also compatible with the data by bremsstrahlung at $E_{max}=2$ GeV.[23]

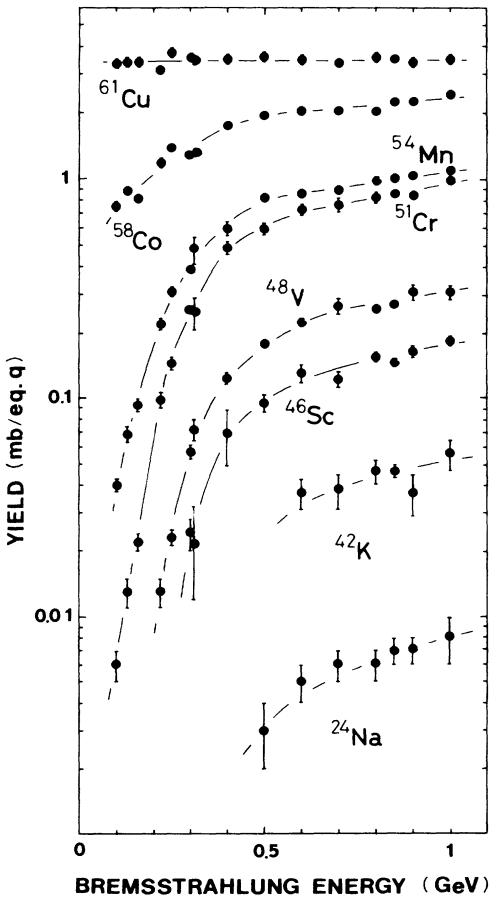

FIG. 2. Excitation functions for individual isotopes that are widely separated in mass.

IV. ANALYSIS AND DISCUSSION

A. Least-squares fit

The spallation yields were fitted by the five-parameter formula, the description of yields in terms of charge distributions and a yield-mass distribution (CDMD), given by Rudstam,[8]

$$\sigma(Z,A)=\frac{\hat{\sigma}PR^{2/3}}{1.79(e^{PA_t}-1)}\exp(PA-R|Z-SA+TA^2|^{3/2}), \tag{1}$$

where $\sigma(Z,A)$ is the yield of a nuclide (Z,A) produced from the target (Z_t,A_t). P, R, S, T, and $\hat{\sigma}$ are free parameters: P defines the slope of the mass yield curve, R the width of the charge dispersion curve, S and T are related to the most probable charge Z_p of the charge dispersion by $Z_p=SA-TA^2$, and $\hat{\sigma}$ is the total inelastic yield. The product mass range used in the analysis was limited to $42 \leqq A \leqq 60$, except for ^{60}Cu, in order to exclude the contribution from other reaction processes such as fragmentation and simple reactions. The yields of ^{57}Co were corrected for the decay of ^{57}Ni. Recently, some modified forms[3–5,24,25] of Rudstam's formula have been used for the analysis. Ku and Karol[26] have analyzed the results of α-induced spallation reactions by applying a skewed Gaussian function to the fitting of the isobaric yield distribution, in order to account for the yields of neutron rich product nuclides. However, we selected the original form of the formula with the symmetric charge distribution in order to compare it with the results calculated by Jonsson and Lindgren,[9,10] who have compiled the parameters for some photospallation yields analyzed by the CDMD formula and proposed relations to calculate the parameters of Rudstam's formula. Among the relations, the expressions for the parameter P,

$$P=1460E_{max}^{-0.81}A_t^{-0.89} \quad \text{for } E_{max} \leqq 600 \text{ MeV}, \tag{2}$$

$$P=7.66A_t^{-0.89} \quad \text{for } E_{max} > 600 \text{ MeV}, \tag{3}$$

are different from that for proton spallation.

The parameters were calculated by a nonlinear least-squares fit to the experimentally obtained spallation yields. The fitting method has been described in detail in Ref. 27, which is basically the same as that suggested by Rudstam.[8] The parameters obtained by this method are given in Table III along with other results of photospallation of Cu.[23,28] The results of the fit at $E_{max}=850$ MeV are shown as an example in Fig. 3. The solid curves were calculated by the formula using the obtained parameter values. It was ascertained that the slope of the mass yield curve and the peak position of the charge dispersion curve are almost independent of fitting methods, although the width of the charge dispersion curve could be somewhat affected by the fitting procedure.

TABLE III. Parameter values for formula (1) obtained from yield data.

E_{max} (MeV)	$\hat{\sigma}$	P	R	S	T
100	58±11	0.69±0.05	2.46±0.10	0.486±0.014	0.000 33±0.000 25
130	51±13	0.58±0.05	2.39±0.14	0.476±0.020	0.000 17±0.000 34
160	36±7	0.50±0.04	2.22±0.12	0.474±0.016	0.000 13±0.000 29
220	34±6	0.39±0.04	2.21±0.13	0.489±0.013	0.000 39±0.000 23
250	37±6	0.35±0.04	2.20±0.13	0.493±0.014	0.000 48±0.000 24
305	26±2	0.26±0.02	2.03±0.09	0.490±0.009	0.000 41±0.000 16
310	26±2	0.25±0.01	2.03±0.11	0.470±0.008	0.000 06±0.000 15
400	32±2	0.21±0.01	2.08±0.08	0.470±0.008	0.000 06±0.000 14
500	38±2	0.19±0.01	1.91±0.09	0.476±0.005	0.000 17±0.000 09
600	39±3	0.17±0.01	2.08±0.11	0.474±0.005	0.000 13±0.000 10
700	41±3	0.18±0.01	2.01±0.10	0.481±0.005	0.000 27±0.000 10
800	40±2	0.16±0.01	1.95±0.08	0.481±0.004	0.000 26±0.000 08
850	42±3	0.16±0.01	2.07±0.09	0.479±0.004	0.000 24±0.000 08
900	44±4	0.16±0.01	1.96±0.10	0.480±0.006	0.000 25±0.000 11
1000	45±3	0.15±0.01	2.07±0.10	0.473±0.005	0.000 11±0.000 09
750[a]		0.21±0.03	1.3 ±0.5	0.48 ±0.02	0.0002±0.0001
2000[b]	72±12	0.16±0.02	2.4 ±0.2	0.478±0.006	0.0002±0.0001

[a]Reference 28.
[b]Reference 23.

B. Slope of mass yield curve

In Fig. 4, the parameter P obtained by the fit is plotted and is slightly lower than the values estimated from the relations (2) and (3), which is shown by the dashed line. However, this result shows the same trend as those from V and I photospallation: P decreases with the increase of the maximum bremsstrahlung energy up to 600 MeV and then approaches a constant value in the higher energy region. In this figure, the slopes of the mass yield curve in proton and heavy ion spallation of Cu obtained by Cumming *et al.*[3–5] are shown by the solid line; the result of α-induced spallation reactions of Cu (Ref. 29) is also included. The parameter P estimated by Rudstam[8] for a number of proton (and some neutron, deuteron, and α)

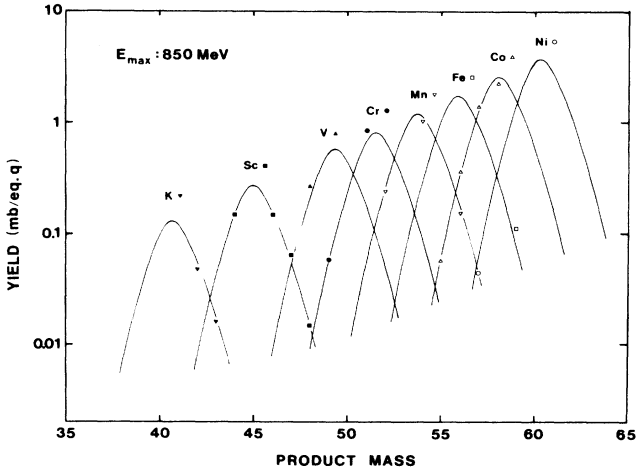

FIG. 3. Yield distributions for products in the mass range $42 \leqq A \leqq 60$ (except for ^{60}Cu) from Cu (γ, spallation) reactions at $E_{max} = 850$ MeV. Solid curves are obtained by the parameters estimated by a nonlinear least-squares fit to the yield data. Open circle denotes Ni, open triangle Co, open square Fe, open inverted triangle Mn, solid circle Cr, solid triangle V, solid square Sc, and solid inverted triangle K.

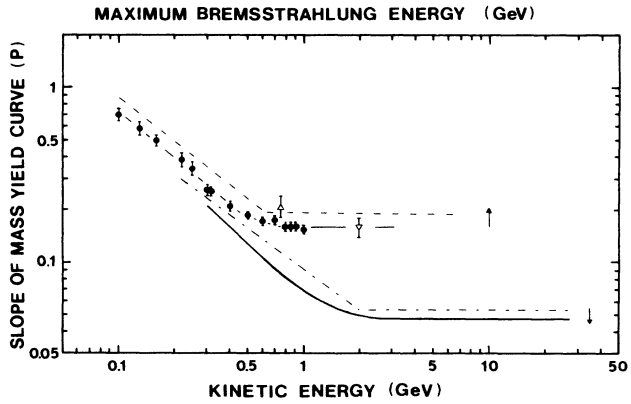

FIG. 4. Logarithmic slope of the mass yield curve (P) as a function of maximum bremsstrahlung energy or kinetic energy of nuclear projectiles. Solid circle denotes this work, open triangle denotes Ref. 28, open inverted triangle denotes Ref. 23. The thin solid curve is to guide the eye for the results of this work. The dashed line was estimated for Cu target from the relations (2) and (3) in the text. The thick solid curve is for the slopes obtained by Cumming *et al.* (Refs. 3–5) for Cu spallation induced by protons and heavy ions (^{14}N, ^{12}C, and ^{40}Ar). Results for α-induced spallation of Cu by Karol (Ref. 29) are also included in this curve. The dash-dotted line is for P values obtained by Rudstam (Ref. 8).

spallation of medium weight target nuclei is indicated by the dash-dotted line. The results by Cumming *et al.*[3–5] and Rudstam[8] are almost consistent with each other. The slopes or P's obtained in hadron spallation of the same target nucleus fall on the same single curve and their values become constant above about 2 GeV. Therefore, two different points comparing photon- and hadron-induced spallations may be deduced.

(1) The slope of the mass yield curve (P) approaches constancy at energies of more than 600 MeV in photospallation, while this constancy is only attained above 2 GeV in hadron spallation.

(2) The slope values of photospallation are larger than those of hadron spallation.

Since the work of photospallation has to depend on bremsstrahlung with a continuous energy spectrum as a photon source, the present results should be converted to those for monochromatic photons. The mean cross sections (mb) in the energy region of 300–1000 MeV were estimated from the yields (mb/eq.q) on the assumption of a $1/E$ dependence of the bremsstrahlung spectrum according to Jonsson and Persson.[7] The parameters obtained for these cross sections were almost identical with those at $E_{max}=600$ and 700 MeV. It does not seem that P decreases to the same value as that of hadron spallation by the conversion of yield to cross section. However, it could be described qualitatively that after conversion the slope (P) would approach a constant value around 600 MeV or less because the mean energy of the interacting photons is less than the maximum end-point energy.

The slope of the mass yield curve is an indirect measure of the energy deposition by the incident particles or photons. From the slope data, the excitation energy seems to saturate at kinetic energies higher than 2 GeV in hadron reactions, but at less than 600 MeV in photon reactions. Furthermore, the comparison shows that the limiting excitation energy is higher in hadron spallation than in photon spallation in this incident energy region. It would seem plausible that the different points (1) and (2) would partly be caused by the difference of the initial interaction between photon and proton spallation because the threshold energy of pion production in photon-nucleon interaction is lower than that in nucleon-nucleon interaction. Further experimental and theoretical investigations are required.

Another support for this discussion is shown in Fig. 5, where the ratios of production yields (mb/eq.q) for photospallation at $E_{max}=850$ MeV to cross sections (mb) for proton spallation at $E_p=3.9$ GeV (Ref. 3) are plotted as a function of product mass number. At these energies, the slope values are constant. It is clearly observed that the yields for photospallation are lower than those for proton spallation and that the ratios decrease with increase of ΔA ($=A_t-A_p$), where A_t and A_p are target and product mass numbers, respectively. The constant ratios among the spallation products would suggest the same distribution of the excitation energies. In fact, it has been reported that the cross section ratios for α to proton spallation of Cu are constant in the same incident energy region, although the absolute cross sections are ~ 1.9 times higher in α spallation than in proton spallation, except for the very neutron deficient products.[29]

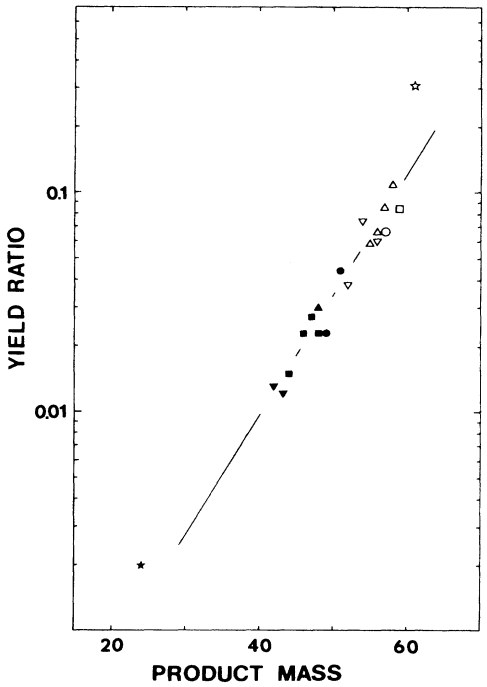

FIG. 5. Isotope ratios of yields (mb/eq.q) for photospallation at $E_{max}=850$ MeV to cross sections (mb) for proton spallation at $E_p=3.9$ GeV as a function of product mass number. Open star denotes Cu, solid star denotes Na. Other symbols are the same as those in Fig. 3.

In pion-induced spallation reactions,[30,31] the slope values plotted as a function of the energy corresponding to the sum of the pion kinetic and rest mass energy show a similar trend as Cumming's solid curve in Fig. 4. The average excitation energy of cascade residues estimated from the slope of the mass yield curve is in the order $\gamma < p = \alpha =$ heavy ion $\fallingdotseq \pi^-$ for the several hundred MeV to several GeV energy region. Therefore, photospallation apparently shows different characteristics than hadron spallation.

The target mass dependence of the slope (P) shown by relations (2) and (3) was also confirmed by our results of photospallation of Y, I, Cs, and Au. These results will be published elsewhere soon.[32]

C. Charge dispersion curve

The charge dispersion curve obtained at $E_{max}=850$ MeV is shown in Fig. 6, as an example. The unmeasured yields of stable and long-lived products were estimated from the CDMD formula by the parameters obtained in this work and all of the yields were converted to relative isobaric yields. In the figure, the curve for 3.9 GeV proton spallation of Cu by Cumming *et al.*[3] is shown by the dashed curve, which is vertically shifted to coincide at the peak position of photospallation. The absolute yields of

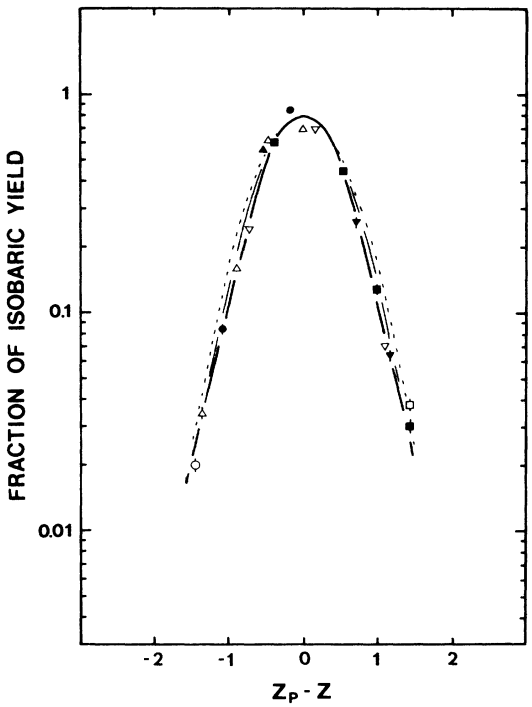

FIG. 6. Charge dispersion curve at $E_{max}=850$ MeV. The symbols are the same as those in Fig. 3. The dashed curve is for 3.9 GeV proton spallation of Cu (Ref. 3), and the thin solid curve is obtained by the analysis of the CDMD-G formula. They are vertically shifted to coincide at the peak position of the thick solid curve obtained by the CDMD formula.

hadron spallation are larger than those of photospallation, and the width of the charge dispersion curve of photospallation is slightly narrower than that of proton spallation. The width of the charge dispersion curve can also be affected by the value of the power of $(Z-SA+TA^2)$. We also performed the analysis using a value of 2 instead of $\frac{3}{2}$ for the power, which corresponds to the CDMD-G (G denotes Gaussian) formula, since Cumming *et al.* used this value. For the value for R, we obtained 1.76 at $E_{max}=850$ MeV, while the other parameter values were identical to those obtained by the CDMD formula. The result for the CDMD-G is shown by the thin solid curve in the figure, which seems to be still narrower than that of proton spallation. If this result is correct, it supports our conclusion about the difference between the average excitation energy of cascade residues of photospallation and hadron reaction described in the preceding section. Unfortunately, these curves overlap with one another for $|Z_p-Z|>1.3$. Therefore, the yields of neutron rich and neutron deficient products must be measured accurately.

D. Most probable charge Z_p

From the parameters S and T, the most probable product N/Z, was estimated by the following relations,

$$Z_p=SA_m-TA_m^2 , \quad (4)$$

$$A_m=A_t-1/P , \quad (5)$$

and was constant within experimental error in the maximum energy region of 100 MeV–1 GeV. An average value of 1.148 ± 0.003 was obtained. The result is shown in Fig. 7 as a function of target N/Z together with those of 1.8 (Ref. 33), 2.9 (Ref. 34), and 12 GeV (Ref. 25) proton and 720 MeV α spallation[26] of targets with various values of N/Z. In this figure, the results obtained by the photospallation of V (Refs. 9 and 10) and I (Ref. 7) are also plotted. These are average values in $E_{max}=100$–800 and 250–1000 MeV, respectively. Furthermore, our data of photospallation of Y, I, Cs, and Au are also shown in the figure. It is found that there exists a nearly linear relationship between target N/Z and the most probable product N/Z in each spallation by photon and proton (and α) and that the slope for photospallation is steeper than that for proton and α spallation. For the larger values of target N/Z, the most probable product N/Z is shifted to the more neutron rich side in photospallation than in proton and α spallation. Solid and dashed lines in the figure, which are to guide the eye, cross around target N/Z of about 1.2. Our result for the most probable product N/Z of the photospallation of Cu agrees well with those of hadron spallation of Cu.[3–5,25,29]

This phenomenon seems to be related to the average excitation energy of cascade residues produced by spallation. At the end of the cascade process, the N/Z ratio of the cascade residues is approximately equal to the target

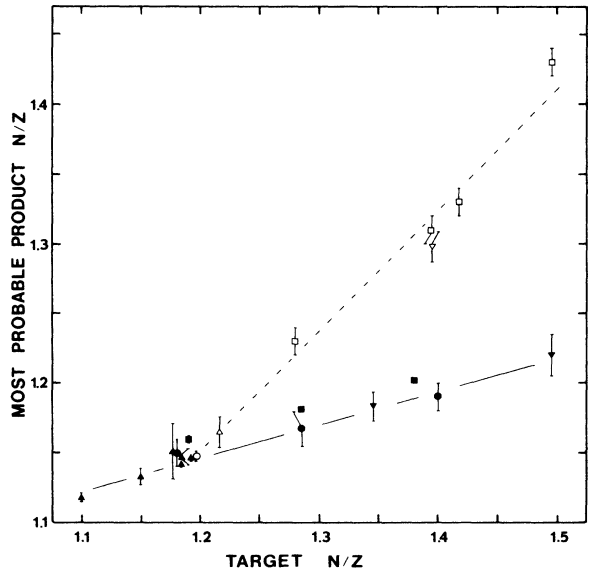

FIG. 7. Most probable product N/Z as a function of target N/Z. Open symbols represent photon results and solid symbols proton and α results. Open circle denotes this work, open triangle Ref. 10 (V target), open inverted triangle Ref. 7 (I), open square Ref. 32 (Y, I, Cs, and Au), solid circle Ref. 34 (^{96}Zr, ^{96}Mo, and ^{96}Ru), solid triangle Ref. 25 (Ti, Fe, Co, Ni, Cu, and Zn), solid inverted triangle Ref. 33 (In and Au), solid square Ref. 26 (^{92}Mo, ^{96}Mo, and ^{100}Mo). The solid and dashed lines are to guide the eye. A portion of the results for proton and α spallation was reproduced from Ref. 26.

N/Z. As the cascade residues are deexcited by evaporation, the Coulomb barrier tends to suppress the emission of protons and charged particles. Since the average excitation energy of cascade residues in photospallation is lower than that in hadron spallation, which is also evidenced by the difference of the parameter P between photon and hadron spallation, the emission of nucleons is relatively limited in photospallation. Therefore, the most probable N/Z is higher in photospallation than in proton and α spallation. Although it is easy to observe this phenomenon in neutron rich target nuclei, it seems to be difficult to see in medium-weight nuclei such as Cu, whose N/Z is near unity.

ACKNOWLEDGMENTS

The authors are indebted to Dr. M. Yagi, Dr. K. Masumoto, and Dr. T. Mitsugashira of Tohoku University; to Dr. T. Tomimasu, Dr. Y. Kawada, and Dr. Y. Hino of ETL; to the operating crew of the synchrotron at INS; and to Dr. K. Yamakoshi of the University of Tokyo for their invaluable cooperation in the accelerator operation and/or the radioactivity measurements.

*Present address: School of Economics, Ottemon-gakuin University, Ibaragi, Osaka 567, Japan.

[1]For example, see *High-Energy Nuclear Reactions in Astrophysics,* edited by B. S. P. Shen (Benjamin, New York, 1967); *Spallation Nuclear Reactions and Their Applications,* edited by B. S. P. Shen (Reidel, Boston, 1976).
[2]R. Serber, Phys. Rev. **72**, 1114 (1947).
[3]J. B. Cumming, P. E. Haustein, R. W. Stoenner, L. Mausner, and R. A. Naumann, Phys. Rev. C **10**, 739 (1974).
[4]J. B. Cumming, R. W. Stoenner, and P. E. Haustein, Phys. Rev. C **14**, 1554 (1976).
[5]J. B. Cumming, P. E. Haustein, T. J. Ruth, and G. J. Virts, Phys. Rev. C **17**, 1632 (1978).
[6]B. Bülow, B. Johnsson, M. Nilsson, and B. Forkman, Z. Phys. A **278**, 89 (1976).
[7]G. G. Jonsson and B. Persson, Nucl. Phys. **A153**, 32 (1970).
[8]G. Rudstam, Z. Naturforsch. **21a**, 1027 (1966).
[9]G. G. Jonsson and K. Lindgren, Phys. Scr. **7**, 49 (1973).
[10]G. G. Jonsson and K. Lindgren, Phys. Scr. **15**, 308 (1977).
[11]K. Sakamoto, H. Toramoto, Y. Hamajima, K. Okada, and M. Dohniwa, Radiochim. Acta **37**, 69 (1984).
[12]K. Sakamoto, M. Nishio, M. Dohniwa, K. Okada and Y. Hamajima, Radiochim. Acta **37**, 83 (1984).
[13]B. Johnsson, A. Järund, and B. Forkman, Z. Phys. A **273**, 97 (1975).
[14]G. Andersson, I. Blomqvist, B. Forkman, G. G. Jonsson, A. Järund, I. Kroon, K. Lindgren, B. Schrøder, and K. Tesch, Nucl. Phys. **A197**, 44 (1972).
[15]G. Kumbartzki, U. Kim, and Ch. K. Kwan, Nucl. Phys. **A160**, 237 (1971).
[16]A. Järund, B. Friberg, and B. Forkman, Z. Phys. **262**, 15 (1973).
[17]A. Masaike, J. Phys. Soc. Jpn., **19**, 427 (1964).
[18]N. di Napoli, A. M. Lacerenza, F. Salvetti, H. G. de Carvalho, and J. Benuzzi-Martins, Lett. Nuovo Cimento **1**, 835 (1971).
[19]G. Hyltén, Nucl. Phys. **A158**, 225 (1970).
[20]T. Nakamura, Nucl. Instrum. Methods **131**, 521 (1975).
[21]*Table of Isotopes,* 7th ed. edited by C. M. Lederer and V. S. Shirley (Wiley, New York, 1978).
[22]K. Komura, Institute for Nuclear Study, University of Tokyo, Technical Report No. INS-TCH 9, 1974 (unpublished).
[23]N. M. Bachschi, P. David, J. Debrus, F. Lübke, H. Mommsen, R. Schoenmackers, G. G. Jonsson, and K. Lindgren, Nucl. Phys. **A264**, 493 (1976).
[24]N. T. Porile, G. D. Cole, and C. R. Rudy, Phys. Rev. C **19**, 2288 (1979).
[25]T. Asano, Y. Asano, Y. Iguchi, H. Kudo, S. Mori, M. Noguchi, Y. Takada, H. Hirabayashi, H. Ikeda, K. Katoh, K. Kondo, M. Takasaki, T. Tominaka, and A. Yamamoto, Phys. Rev. C **28**, 1718 (1983).
[26]T. H. Ku and P. J. Karol, Phys. Rev. C **16**, 1984 (1977).
[27]Y. Kubota, M.S. thesis, Kanazawa University, 1986 (unpublished).
[28]The data were cited in Ref. 7 as G. G. Jonsson, preliminary results.
[29]P. J. Karol, Phys. Rev. C **10**, 150 (1974).
[30]P. E. Haustein and T. J. Ruth, Phys. Rev. C **18**, 2241 (1978).
[31]T. Nishi, I. Fujiwara, N. Imanishi, H. Moriyama, K. Otozai, R. Arakawa, T. Saito, T. Tsuneyoshi, N. Takahashi, S. Iwata, S. Hayashi, S. Shibata, H. Kudo, and K. Yoshida, Bull. Inst. Chem. Res., Kyoto Univ. **60**, 132 (1982).
[32]K. Sakamoto, Y. Hamajima, M. Soto, Y. Kubota, M. Yoshida, T. Hashimoto, T. Fukasawa, I. Fujiwara, and S. Shibata, Laboratory of Nuclear Science, Tohoku University, Research Report No. 18, p. 290, 1985 (unpublished).
[33]S. Kaufman, Phys. Rev. **129**, 1866 (1963).
[34]N. T. Porile and L. B. Church, Phys. Rev. **133**, B310 (1964).